[6] Flugge, W., *Stresses in Shells* (Springer-Verlag, Berlin, 1962).
[7] Green, A. and Zerne, W., *Theoretical Elasticity* (Oxford University Press, London, 1954).
[8] Jenkinsen, P. M., McAlister, R. H., Lutz, J. F., and Kuenzi, E. W., "Evaluation of plywood cylindrical shells subjected to external radial pressure," Forest Products Lab. Rept. PE-224 (October 1961).
[9] Sokolnikoff, I. S., *Mathematical Theory of Elasticity* (McGraw-Hill Book Co. Inc., New York, 1956).
[10] Sokolnikoff, I. S., *Tensor Analysis* (John Wiley and Sons Inc., New York, 1951).
[11] Stanton, R. G., *Numerical Methods for Science and Engineering* (Prentice-Hall Inc., Englewood Cliffs, N. J., 1961).
[12] March, H. W., Norris, C. B., Smith, C. B., and Kuenzi, E. W., "Buckling of thin-walled plywood cylinders in torsion," Forest Products Lab. Rept. 1529 (June 1945).

JULY 1963 AIAA JOURNAL VOL. 1, NO. 7

Plastic Instability of Cylindrical Pressure Vessels of Finite Length

P. MANN-NACHBAR,* O. HOFFMAN,† AND W. E. JAHSMAN†

Lockheed Missiles and Space Company, Sunnyvale, Calif.

A mathematical analysis is given for the plastic instability of an internally pressurized cylindrical shell of finite length. The ends of the shell are free to rotate and to translate axially but are restrained from radial motion. Tresca's yield condition and the associated flow rule are used, and the shell material obeys Ludwik's power law, $\sigma_e = C(\epsilon_e)^n$, where σ_e and ϵ_e are the effective stress and strain, and C and n are material constants. When the deformed shape of the meridian of the pressurized shell can be represented by a parabola, the instability pressure increases from the known value for long shells to approximately twice that value for short shells. The bulk of the increase in the instability pressure occurs for the shells with length less than diameter. For fixed shell length, the instability pressure increases with increasing values of the strain-hardening exponent n.

Introduction

UNTIL recently, studies of plastic tension instability have dealt with rather simple structural elements such as rods, plates, and infinite cylinders.[1] In particular, the effects of end constraints have not been considered. Within the past two years, however, two independent reports have appeared which deal with the strengthening effect of end constraints on the plastic instability of internally pressurized cylinders of finite length, the ends of which are restrained against radial motion.[2, 3] These reports show that, as the length-to-diameter ratio of the cylinder decreases toward unity, the instability pressure, i.e., the local maximum of the pressure function $p = p(\epsilon_e)$, increases slightly, usually by less than 10%. Below length-to-diameter ratios of unity, these solutions cease to be valid because the total strain (or deformation) theory of plasticity is used in the analyses. As is well known, this theory applies only for nearly constant stress ratios, and it is shown in Ref. 2 that this condition generally requires length-to-diameter ratios greater than unity.

In the present paper, the incremental (or flow) theory of plasticity is used, and no limitations on length-to-diameter ratios appear. A complete range of dependence of the instability pressure on length-to-diameter ratios ranging from zero to infinity is developed. For some ranges of length-to-diameter ratios, two instability pressures (i.e., two local pressure maxima) are found, with the larger instability pressure occurring at rather large deformations. If the cylinder material has limited ductility, the smaller instability pressure may govern; otherwise, failure will occur at the larger instability pressure. Final results give both instability pressures, so that the range of possible failure pressures is available. It is found that the ends of the cylinder have a pronounced strengthening effect when the length is less than the diameter. This trend also is observable in published experimental data.[4]

Presented at the IAS 31st Annual Meeting, New York, January 20–23, 1963; revision received May 10, 1963.

* Staff Scientist, Mechanical and Mathematical Sciences Laboratory.
† Senior Staff Scientist, Mechanical and Mathematical Sciences Laboratory.

Basic Equations

A cylindrical pressure vessel of initial radius R and length $2L$ has end supports that permit meridional rotation and axial extension but prevent radial motion. Under pressurization, the vessel will "barrel out" and change length as shown in Fig. 1. Equilibrium of the deformed cylinder is governed by the membrane relations

$$\sigma_\phi = pr_2/2h \tag{1}$$

$$\sigma_\theta = (pr_2/2h)[2 - (r_2/r_1)] \tag{2}$$

where σ_ϕ and σ^θ are the meridional and circumferential membrane stresses,‡ p is the internal pressure, h is the instantaneous wall thickness, and r_1 and r_2 are the principal radii of curvature shown in Fig. 2. The radius r_1 lies in the meridional plane and is related to the instantaneous distance from the shell to the axis r by

$$r_1 = -(1 + r'^2)^{3/2}/r'' \tag{3}$$

whereas the radius r_2 lies in the plane perpendicular to the

‡ As usual, the transverse normal stress σ_r is neglected in comparison with σ_ϕ and σ_θ.

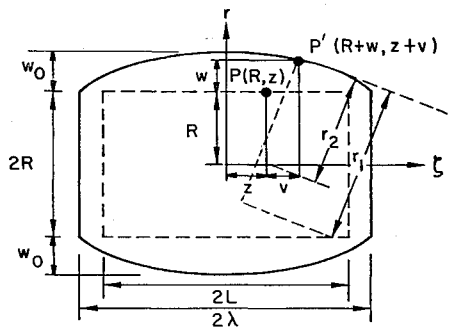

Fig. 1 Initial and deformed geometry of cylindrical vessel

meridional and tangent planes and is related to r by

$$r_2 = r(1 + r'^2)^{1/2} \tag{4}$$

Primes in Eqs. (3) and (4) and in what follows denote differentiation with respect to the axial coordinate ζ (see Fig. 1).

Since the strains may be large, the logarithmic measure is used. Thus, the meridional, circumferential, and transverse normal strains are given by

$$\epsilon_\phi = \ln(ds/dz) = \ln(1 + r'^2)(d\zeta/dz) \tag{5}$$

$$\epsilon_\theta = \ln(r/R) \tag{6}$$

$$\epsilon_r = \ln(h/H) \tag{7}$$

where, as shown in Fig. 1, (R, z) and (r, ζ), respectively, are the coordinates of a material particle before and after deformation, the point (0,0) coinciding with the center of the cylinder. The quantity s represents the distance along the meridian from the equatorial plane, and H is the original thickness of the cylinder wall.

The cylinder material is assumed to be rigid-plastic and to obey Ludwik's power law of strain hardening and the Tresca yield condition. Ludwik's law requires a unique relationship between σ_e and ϵ_e, taken here as the power relation§

$$\sigma_e = C\epsilon_e^n \tag{8}$$

where σ_e and ϵ_e are the "effective stress" and "effective strain" and are defined, respectively, by

$$\sigma_e = |\sigma_{\max} - \sigma_{\min}| \tag{9}$$

$$\epsilon_e = \tfrac{2}{3} \int |d\epsilon_{\max} - d\epsilon_{\min}| \tag{10}$$

In Eqs. (9) and (10), $\sigma_{\max}$ and $\sigma_{\min}$ and $d\epsilon_{\max}$ and $d\epsilon_{\min}$ are the algebraically largest and smallest principal stresses and strain increments, respectively, and C and n are material constants. The factor $\frac{2}{3}$ in Eq. (10) assures that the longitudinal-stress/longitudinal-strain relation in simple tension or simple compression becomes identical with the effective-stress/effective-strain relation.

Since the meridional and circumferential directions are the principal directions of stress and strain, Eq. (9) for the Tresca yield condition may be illustrated as shown in Fig. 2. For convenience, σ_ϕ and σ_θ are normalized with respect to the instantaneous values of σ_e. It is seen that the yield condition is represented by the hexagon $ABCDEFA$ in the $(\sigma_\theta/\sigma_e, \sigma_\phi/\sigma_e)$ plane. In such a representation, a straight line issuing from the origin is the locus of points of constant $\sigma_\phi/\sigma_\theta$ and, by virtue of Eqs. (1) and (2), the locus of points of constant r_2/r_1. For example, in an infinitely long internally pressurized cylinder where $r_2/r_1 = 0$, point G, with $\sigma_\phi/\sigma_\theta = \frac{1}{2}$, represents the state of stress throughout the shell. This condition prevails also in finite-length cylinders for small internal pressure. With increasing pressure, however, $r_2/r_1 > 0$, so that $\sigma_\phi/\sigma_\theta > \frac{1}{2}$, and the state of stress is represented by points that move along the hexagon from G to B and possibly toward C.

For the stress ratios between G and B, $\sigma_\theta/\sigma_e = 1$, i.e., the effective stress is the circumferential stress, σ_θ. The incompressibility condition and the flow rule associated with Tresca's yield condition furnish the strain-increment ratios

$$d\epsilon_\phi : d\epsilon_\theta : d\epsilon_r = 0 : \tfrac{1}{2} : -\tfrac{1}{2} \tag{11}$$

By virtue of Eq. (9), the effective strain becomes

$$\epsilon_e = \tfrac{2}{3} \int |d\epsilon_\theta - d\epsilon_r| = \tfrac{4}{3}\epsilon_\theta \tag{12}$$

and from Eq. (11), the total strains may be written as

$$\epsilon_\phi = 0 \tag{13}$$

$$\epsilon_r = -\epsilon_\theta \tag{14}$$

Equations (11–14) are valid until the corner B is reached. There the strain-increment ratio $d\epsilon_\phi : d\epsilon_\theta$ takes on some positive although indeterminate value, whereas the principal stresses are equal ($\sigma_\phi = \sigma_\theta = \sigma_e$). Whether instability occurs before or after the corner is reached depends on the strain-hardening parameter n and the length-radius ratio L/R. It will be found that, for values of n commonly encountered in high-strength rocket motor case materials, i.e., $n < 0.1$, instability occurs before the corner is reached if the cylinder is long ($L/R > 1$). If the cylinder is short ($L/R < 1$), instability occurs at a stage of deformation associated with the corner B or the side BC.

Formally, the problem is defined by Eqs. (1–10) together with the appropriate boundary conditions and a knowledge (known a priori or assumed and verified a posteriori) of the stress ratio to determine the location on the yield diagram (Fig. 2). For example, when the stress ratios fall along GB, Eqs. (11–14) apply. These and the preceding equations may be combined to yield a single, nonlinear, second-order differential equation in $r(\zeta)$. Rather than attempt to obtain a general solution for $r(\zeta)$, we will assume that the shape of the meridian curve is well approximated by a parabola, i.e., we take

$$r = R + w_0(1 - \zeta^2/\lambda^2) \tag{15}$$

where w_0 is the radial displacement at the equator and λ is related to L, the original half-length of the cylinder, through

$$L = \int_0^\lambda e^{-\epsilon_\phi}(1 + r'^2)^{1/2} d\zeta \tag{16}$$

derivable directly from Eq. (5). This choice for the meridian curve recommends itself by its plausibility and simplicity. Moreover, it is shown in the Appendix that for small deformations the meridian shape is approximately parabolic.

In the subsequent discussion of the instability of the finite cylinder, the conditions under which failure can occur along the equator of the deflected shell will be examined. The justification for having confined our attention to this region lies primarily in an intuitive reasoning that associates the improved behavior of the finite cylinder with the reinforcing effect of the end constraints and presumes that the area that is most remote from the ends, i.e., the area of the equator, is the critical one.

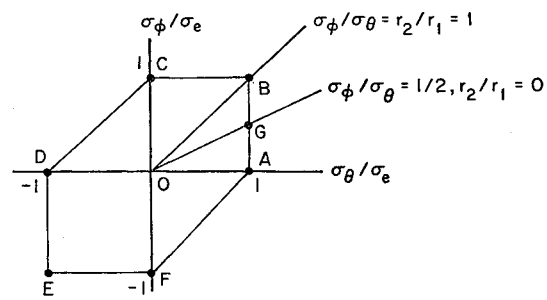

Fig. 2 Tresca's yield condition

§ Use of this relation should not be interpreted as using total strain theory, c.f. Eq. (10), which defines ϵ_e.

The radius ratio $(r_2/r_1)_{\zeta=0}$, which determines the position on the yield hexagon, is obtained by combining Eqs. (3, 4, and 15):

$$(r_2/r_1)_{\zeta=0} = 2w_0(R + w_0)/\lambda^2 \tag{17}$$

It may be shown that (r_2/r_1) takes on its largest value at $\zeta = 0$. Hence, the corner B in Fig. 2, for which the stress ratio $\sigma_\phi/\sigma_\theta = 1$ and the radius ratio $r_2/r_1 = 1$, is reached first at points on the equator. At this instant, the deflection w_0 assumes the particular value

$$w_0^* = (R/2)\{[1 + 2(\lambda^{*2}/R^2)]^{1/2} - 1\} \tag{18}$$

and the total strains at the equator become, with reference to Eqs. (6, 13, and 14),

$$\epsilon_{\theta_0}^* = \ln\tfrac{1}{2}\{[1 + 2(\lambda^{*2}/R^2)]^{1/2} + 1\} = -\epsilon_{r_0}^* \tag{19}$$

$$\epsilon_{\phi_0}^* = 0 \tag{20}$$

The following analysis will deal separately with two distinct stages of deformation of the vessel. In the first stage ($w_0 < w_0^*$), Eqs. (11–14) apply. In the second stage ($w_0 \geqq w_0^*$), when the state of stress has reached the corner B of the Tresca hexagon, altogether different relationships apply, and these will be developed as they are needed later in the analysis.

First Stage of Vessel Deformation

A state of plastic instability is defined to exist when the function $p = p(\epsilon_e)$ reaches a maximum. Because of Eq. (12), it is sufficient to examine p as a function of ϵ_θ.

The internal pressure p can be written readily as an explicit function of ϵ_θ. Equations (2–4, 6, 7, 14, and 15) yield, at the equator,

$$p = \frac{H}{R} e^{-2\epsilon_{\theta_0}} \left[\frac{1}{1 - (R/\lambda)^2(e^{\epsilon_{\theta_0}} - 1)\, e^{\epsilon_{\theta_0}}}\right] \sigma_{\theta_0} \tag{21}$$

The circumferential stress and strain, σ_θ and ϵ_θ, now may be related directly by making use of the quantities σ_e and ϵ_e. It will be recalled that in the first stage of deformation $\sigma_\theta = \sigma_e$, and from Eq. (12), $\frac{4}{3}\epsilon_\theta = \epsilon_e$. Hence, by Eq. (10),

$$\sigma_\theta = C(\tfrac{4}{3})^n \epsilon_\theta^n \tag{22}$$

and Eqs. (21) and (22) combine to form

$$p = C\frac{H}{R}\left(\frac{4}{3}\right)^n \left\{\frac{e^{-2\epsilon_{\theta_0}}(\epsilon_{\theta_0})^n}{1 - (R/\lambda)^2(e^{\epsilon_{\theta_0}} - 1)e^{\epsilon_{\theta_0}}}\right\} \tag{23}$$

Typical behavior of this pressure function is shown in Fig. 3. The range of ϵ_{θ_0} is from 0 to $\epsilon_{\theta_0}^*$, where $\epsilon_{\theta_0}^*$ is given by Eq. (19) and represents the value of ϵ_{θ_0} at which the corner B of the Tresca hexagon is reached. It is seen that p at first increases with ϵ_{θ_0}, reaches a local maximum, dips to a local minimum, and then begins to increase again as $\epsilon_{\theta_0}^*$ is approached. The local maximum represents the instability pressure p_i. The factor R/λ in the denominator of Eq. (23) varies with ϵ_{θ_0}, the functional relationship being given by Eq. (16) with $\epsilon_\phi = 0$. It can be shown, however, that

$$R/\lambda = (R/L)[1 + \tfrac{2}{3}\epsilon_{\theta_0}^2 + 0(\epsilon_\theta^3)]$$

The analysis will be much simplified if one writes $R/\lambda = R/L$, or

$$p = C\frac{H}{R}\left(\frac{4}{3}\right)^n \left\{\frac{e^{-2\epsilon_{\theta_0}}(\epsilon_{\theta_0})^n}{1 - (R/L)^2(e^{\epsilon_{\theta_0}} - 1)e^{\epsilon_{\theta_0}}}\right\} \tag{24}$$

This is equivalent to neglecting terms of order $(R^2/L^2)\epsilon_{\theta_0}^3$ in comparison with terms of order 1 in the denominator of Eq. (23). It will be seen shortly that the restriction $(R^2/L^2)\epsilon_{\theta_0}^3 \ll 1$ actually does not limit the usefulness of the analysis.

Stationary points for p as given by Eq. (24) can be found by straightforward differentiation. The condition $dp/d\epsilon_{\theta_0} = 0$ implies that, at a relative maximum or minimum, ϵ_{θ_0} must satisfy the equation

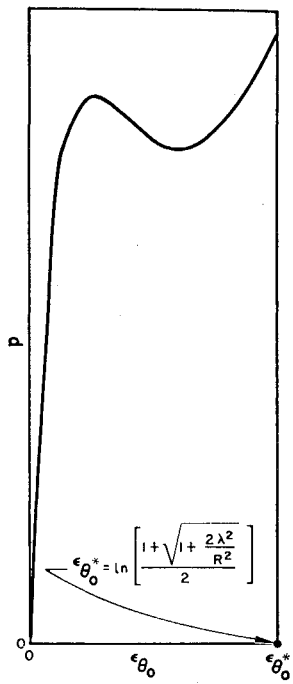

Fig. 3 The pressure function; first stage of deformation

$$\frac{2\epsilon_{\theta_0}}{n} = \frac{1 - (R^2/L^2)(e^{2\epsilon_{\theta_0}} - e^{\epsilon_{\theta_0}})}{1 - (R^2/L^2)(e^{2\epsilon_{\theta_0}} - \frac{3}{4}e^{\epsilon_{\theta_0}})} \tag{25}$$

This equation can be solved quite easily either numerically or graphically. Once the instability strain is known, the instability pressure can be computed from Eq. (24). In the present study, instability strains ϵ_{θ_0}, and instability pressures p_i were found for $0.005 \leq n \leq 0.1$ and $L/R \gtrsim 1$.

Results are presented in Fig. 4 as curves of $\bar{p}_i$ vs L/R for several values of n. The normalized instability pressure $\bar{p}_i$ is the ratio of p_i at a particular L/R to p_i at $L/R \to \infty$. As obtained previously (for example, see Ref. 1),

$$p_i \xrightarrow[L/R\to\infty]{} \frac{CH}{R}\left(\frac{2}{3}\right)^n \left(\frac{n}{e}\right)^n$$

It is seen that, for any strain-hardening exponent n, the instability pressure increases as the cylinder is shortened, demonstrating the strengthening effect of the fixed ends.

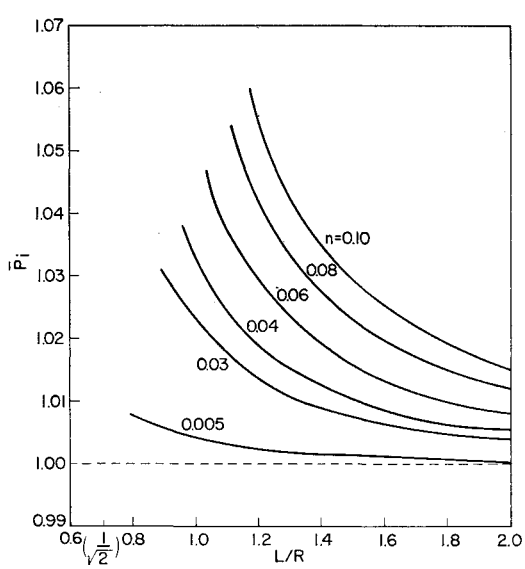

Fig. 4 Pressure ratios at instability; first stage of deformation

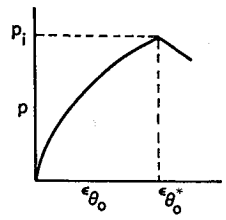

Fig. 5 Pressure function during transition from stage 1 to stage 2

These curves are in excellent agreement with those found previously in Refs. 2 and 3.

It will be recalled that the leading neglected term in Eq. (23) was $(R^2/L^2)\epsilon_{\theta_0}{}^3$. For the values of n of interest here, $(R^2/L^2)\epsilon_{\theta_0}{}^3 < 0.005$, and there is no significant difference in behavior between Eqs. (23) and (24).

The termination of the curves near $L/R = 1$ is caused by the disappearance of the local maximum in Fig. 3.‖ For given n, as L/R decreases, the local maximum and minimum in Fig. 3 approach each other and eventually merge to an inflection point. Below this critical value of L/R, no stationary values exist in the range $0 \leq \epsilon_{\theta_0} \leq \epsilon_{\theta_0}{}^*$. Thus, behavior of the pressure function during the second stage of deformation (at or beyond the corner B of the Tresca hexagon) must be examined for instability.

Second Stage of Vessel Deformation: Shells of Intermediate Length

The shell enters the second stage of deformation when Eqs. (18–20) hold. Since there are equal radii of curvature at the equator,

$$\sigma_{\phi_0} = \sigma_{\theta_0} = \sigma_{e_0} \tag{26}$$

A relation between pressure and strain may be obtained by combining Eqs. (1, 4, 6–8, 15, and 26) and then using the incompressibility condition to form

$$p = 2(HC/R)(\epsilon_{e_0})^n e^{-(2\epsilon_{\theta_0}+\epsilon_{\phi_0})} \tag{27}$$

At the corner of the Tresca hexagon, the flow rule no longer furnishes a relationship between the strain increments $d\epsilon_\theta$ and $d\epsilon_\phi$ except to require that they be nonnegative. However, considerable information can be obtained without any knowledge of the behavior of the strain-rate vector. It turns out that, for a wide range of L/R values, instability occurs as soon as the corner is reached, and that the instability pressures and strains are then independent of even the initial direction of the strain-rate vector.

Call the initial value of $d\epsilon_{\phi 0}/d\epsilon_{\theta 0}$ at the corner of the Tresca hexagon β^*, i.e.,

$$\left.\frac{d\epsilon_{\phi_0}}{d\epsilon_{\theta_0}}\right]_{\substack{\epsilon_{\phi_0}=0 \\ \epsilon_{\theta_0}=\epsilon_{\theta_0}{}^* \\ \epsilon_{e_0}=\epsilon_{e_0}{}^*=(4/3)\epsilon_{\theta_0}{}^*}} = \beta^* \geq 0$$

$\beta^* \geq 1$ corresponds to $d\epsilon_{\phi_0} \geq d\epsilon_{\theta_0}$ and implies that initially

$$d\epsilon_{e_0} = \tfrac{2}{3}(d\epsilon_{\phi 0} - d\epsilon_{r_0})$$

or, because of incompressibility,

$$d\epsilon_{e_0} = \tfrac{2}{3}(2d\epsilon_{\phi_0} + d\epsilon_{\theta_0}) \tag{28}$$

If, on the other hand, $\beta^* \leq 1$, then initially

$$d\epsilon_{e_0} = \tfrac{2}{3}(d\epsilon_{\phi_0} + 2d\epsilon_{\theta_0}) \tag{29}$$

Consider first that $\beta^* \geq 1$, and that, in some small region of the $(\epsilon_{\phi_0}, \epsilon_{\theta_0})$ plane, the ordering of strain rates remains as

$$d\epsilon_{\phi_0} \geq d\epsilon_{\theta_0} > d\epsilon_{r_0}$$

that is,

$$d\epsilon_{\phi_0}/d\epsilon_{\theta_0} = \beta^* + F(\epsilon_{\theta_0}, \epsilon_{\phi_0}) \geq 1 \tag{30}$$

where $F(\epsilon_{\theta_0}{}^*, 0) = 0$.

The effective strain, which can be written as

$$\epsilon_{e_0} = \int_0^{\epsilon_{\theta_0}{}^*} d\epsilon_{e_0} + \int_{\epsilon_{e_0}{}^*}^{\epsilon_{e_0}} d\epsilon_{e_0}$$

reduces, because of Eq. (28), to

$$\epsilon_{e_0} = \tfrac{4}{3}\epsilon_{\phi_0} + \tfrac{2}{3}(\epsilon_{\theta_0} + \epsilon_{\theta_0}{}^*) \tag{31}$$

The strains ϵ_{ϕ_0} and ϵ_{θ_0} are related through Eq. (30). At least in principle, Eq. (31) permits the effective strain to be written as a function (increasing) of ϵ_{θ_0} (or ϵ_{ϕ_0}) alone. Conditions for instability therefore can be determined by examining the behavior of p as a function of ϵ_{θ_0} (or ϵ_{ϕ_0}).

Since one is looking for relative maxima, consider the first derivative of Eq. (27):

$$\frac{dp}{d\epsilon_{\theta_0}} = \frac{4}{3}\frac{HC}{R}\left[\frac{4}{3}\epsilon_{\phi_0} + \frac{2}{3}(\epsilon_{\theta_0} + \epsilon_{\theta_0}{}^*)\right]^{n-1} e^{-(2\epsilon_{\theta_0}+\epsilon_{\phi_0})} \times$$

$$\left\{n\left(2\frac{d\epsilon_{\phi_0}}{d\epsilon_{\theta_0}} + 1\right) - (2\epsilon_{\phi_0} + \epsilon_{\theta_0} + \epsilon_{\theta_0}{}^*)\left(2 + \frac{d\epsilon_{\phi_0}}{d\epsilon_{\theta_0}}\right)\right\} \tag{32}$$

Initially

$$\left.\frac{dp}{d\epsilon_{\theta_0}}\right]_{\substack{\epsilon_{\theta_0}=\epsilon_{\theta_0}{}^* \\ \epsilon_{\phi_0}=0}} = \frac{4}{3}\frac{HC}{R}\left[\frac{4}{3}\epsilon_{\theta}{}^*\right]^{n-1} e^{-2\epsilon_{\theta_0}{}^*} \times$$

$$\{n(2\beta^* + 1) - 2\epsilon_{\theta_0}{}^*(2 + \beta^*)\} \tag{33}$$

The behavior of p is illustrated in Fig. 5.

Generally, there will be a discontinuity in slope at the onset of the second stage of deformation. Because of this, it is possible to have a relative maximum, and therefore instability, even though the condition $dp/d\epsilon_{\theta_0} = 0$ cannot be satisfied.

If

$$\epsilon_{\theta_0}{}^* \geq \frac{n}{2}\frac{2\beta^* + 1}{2 + \beta^*} \tag{34}$$

the slope starts out negative or zero in the second stage, and instability occurs as soon as the shell becomes locally spherical at the equator. If

$$\epsilon_{\theta_0}{}^* < \frac{n}{2}\frac{2\beta^* + 1}{2 + \beta^*} \tag{35}$$

the slope starts out positive, and instability presumably occurs for some $\epsilon_{\theta_0} > \epsilon_{\theta_0}{}^*$.

The situation is similar but even simpler for $\beta^* \leq 1$. In this case, because of Eq. (29), the effective strain becomes

$$\epsilon_{e_0} = \tfrac{2}{3}(2\epsilon_{\theta_0} + \epsilon_{\phi_0}) \tag{36}$$

The pressure therefore can be written explicitly as a function of ϵ_{e_0}. From Eqs. (27) and (36),

$$p = 2(HC/R)(\epsilon_{e_0})^n e^{-(3/2)\epsilon_{e_0}} \tag{37}$$

and the derivative with respect to effective strain has the form

$$dp/d\epsilon_{e_0} = 2(HC/R)\epsilon_{e_0}{}^{n-1}e^{-(3/2)\epsilon_{e_0}}[n - \tfrac{3}{2}\epsilon_{e_0}] \tag{38}$$

Since, initially, $\epsilon_{e_0} = \epsilon_{e_0}{}^* = \frac{4}{3}\epsilon_{\theta_0}{}^*$, it follows from Eq. (38) that for $\beta^* \leq 1$ the slope will start out negative or zero in the second stage whenever $\epsilon_{\theta_0}{}^* \geq n/2$.

‖ The termination does not result from the approximation $R/\lambda \approx R/L$ introduced into Eq. (23). In fact, it can be proved that the L/R values at which stationary points begin to disappear are slightly greater for Eq. (23) than for Eq. (24).

The right-hand side of Eq. (34) increases from $n/2$ to n as β^* increases from 1 to $+\infty$. Therefore, at least for

$$\epsilon_{\theta_0}{}^* \geq n \tag{39}$$

instability occurs as soon as the corner of the Tresca hexagon is reached, for all values of β^*.

The instability pressure ratio $\bar{p}_i$ is computed easily. Since the instability strains have the values

$$\begin{aligned} \epsilon_{\theta_{0i}} &= \epsilon_{\theta_0}{}^* & \epsilon_{\phi_{0i}} &= 0 \\ \epsilon_{r_{ci}} &= -\epsilon_{\theta_0}{}^* & \epsilon_{e_{0i}} &= \tfrac{4}{3}\epsilon_{\theta_0}{}^* \end{aligned} \tag{40}$$

Eq. (27) yields

$$p_i = 2(HC/R)(\tfrac{4}{3}\epsilon_{\theta_0}{}^*)^n e^{-2\epsilon_{\theta_0}{}^*}$$

Therefore

$$\bar{p}_i = 2(2e/n)^n(\epsilon_{\theta_0}{}^*)^n e^{-2\epsilon_{\theta_0}{}^*} \tag{41}$$

The strain $\epsilon_{\theta_0}{}^*$ depends only on L/R [through Eqs. (16) and (19)]. For $n = 0.04$, Eq. (39) will be satisfied for all $L/R > \sim 0.25$; for $n = 0.10$, Eq. (36) requires that $L/R > \sim 0.35$. For quite a wide range of parameter values, then, the instability strains and pressures can be determined without considering the direction of the strain-increment vector at the corner of the Tresca hexagon.

Normalized instability pressures calculated from Eq. (41) with the aid of Eqs. (16) and (19) are plotted in Fig. 6 for $n = 0.04$ and $n = 0.10$. Also shown are the appropriate "long-cylinder" curves from Fig. 4. The strengthening effect of the ends is very much in evidence. The tendency of the instability pressure to increase as the shell length decreases, mildly exhibited by the "long cylinders," is confirmed strongly. For example, as L/R decreases from $\sim$1.5 to $\sim$0.5, the instability pressure almost doubles.

Figure 6 shows that, when $L/R \gtrsim 1$, two instability pressures are predicted. This phenomenon may be explained by recalling that the instability pressures represent local maxima in the deformation process. Thus, the pressure function, after reaching a relative maximum during the first stage, continues to increase until a second relative maximum is reached at the onset of the second stage. The strains associated with the second maximum are quite large, $\epsilon_{\theta_0}{}^*$ ranging from 26% at $L/R = 0.96$, and $n = 0.04$ to over 50% at $L/R = 1.60$, $n = 0.10$. If the cylinder material has limited ductility, the instability pressure associated with the first stage of deformation will govern. In any event, the lower curve is conservative and represents a lower bound to the instability pressure. Use of the lower curve leaves a discontinuous transition from first- to second-stage instability pressures at certain critical L/R values. For example, when $n = 0.04$, the dimensionless instability pressure increases from 1.04 at $L/R = 0.96+$ to 1.36 at $L/R = 0.96-$. This behavior reflects the fact that, for points on the first-stage curve in Fig. 6, the values of the circumferential strains and pressures at instability are well below the corresponding values at which the cyclinder enters the second stage. Immediately to the left of the transition points, where there is

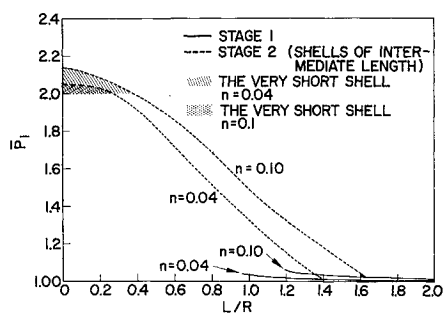

Fig. 6 Pressure ratios at instability

only one instability pressure, the circumferential strains are large, e.g., 25% for $L/R = 0.95$. As L/R decreases, however, the strains decrease, so that the second-stage curve is expected to govern for sufficiently short cylinders.

The Very Short Shell

Those shells still must be considered for which $\epsilon_{\theta_0}{}^* < n$, or, more precisely, shells for which

$$\epsilon_{\theta_0}{}^* < n/2 \quad \text{if} \quad \beta^* \leq 1 \tag{42}$$

or

$$\epsilon_{\theta_0}{}^* < \frac{n}{2}\left[\frac{2\beta^* + 1}{\beta^* + 2}\right] \quad \text{if} \quad \beta^* \geq 1 \tag{43}$$

For values of n considered here, shells with $\epsilon_{\theta_0}{}^* < n$ are so short that they more properly should be called rings. It is doubtful whether they can be represented adequately by the mathematical model described in the section on basic equations. A brief discussion of their instability will be included, however, for completeness and to illustrate the behavior of the model for vanishingly small values of L/R.

It will be recalled that, if the inequalities in Eqs. (42) and (43) are satisfied, then the slope of the pressure vs strain curve starts out positive in the second stage of deformation. To discuss stability, it then is necessary to consider the pattern of deformation *after* the corner of the Tresca hexagon has been reached and, in particular, to consider the behavior of the strain-increment vector at the corner.

If instability occurs shortly, although not immediately, after the shell enters the second stage of deformation, so that one may approximate $d\epsilon_{\phi_0}/d\epsilon_{\theta_0}$ by its initial value,# i.e.,

$$d\epsilon_{\theta_0}/d\epsilon_{\theta_0} \approx \beta^* \geq 0 \tag{44}$$

and if the deformation is such that one continues to have

$$r_2/r_1]_{\zeta=0} \geq 1$$

then it can be shown that, for small n, the dependence of the instability pressure on β^* is slight, and that, for all β^*, $\bar{p}_i \approx 2$.

If $r_2/r_1]_{\zeta=0} \geq 1$, then $\sigma_{\varphi_0} \geq \sigma_{\theta_0}$ and, accordingly, $\sigma_{e_0} = \sigma_{\varphi_0}$. If, in addition, the strain-rate vector maintains a constant direction as stipulated, then much of the development of the foregoing section, previously applied only at the initial point $\epsilon_{\varphi_0} = 0$, $\epsilon_{\theta_0} = \epsilon_{\theta_0}{}^*$, remains valid as the shell continues to deform.

Consider first $\beta^* \geq 1$. For these β^* values, Eqs. (27, 28, 31, and 32) continue to apply. Since $\epsilon_{\varphi_0} = \beta^*(\epsilon_{\theta_0} - \epsilon_{\theta_0}{}^*)$, the condition $dp/d\epsilon_{\theta_0} = 0$ yields**

$$\epsilon_{\theta_{0i}} = n\left[\frac{1}{2 + \beta^*}\right] + \left[\frac{2\beta^* - 1}{2\beta^* + 1}\right] \tag{45}$$

and by direct substitution and simple manipulation the instability pressure ratio is found to be

$$\bar{p}_i = 2\left[\frac{2\beta^* + 1}{2 + \beta^*}\right]^n e^{-\epsilon_{\theta_0}{}^*[(2\beta^* - 2)/(2\beta^* + 1)]} \tag{46}$$

If now $\beta^* \leq 1$, the pressure and its first derivative are given by Eqs. (37) and (38). The condition $dp/d\epsilon_{e_0} = 0$ yields††

$$\epsilon_{e_{0i}} = \tfrac{2}{3}n \tag{47}$$

Relaxation of this requirement does not appear feasible at present.

** Note that, since $\epsilon_{\theta_0}{}^* < (n/2)[(2\beta^* + 1)/(\beta^* + 2)]$, then $\epsilon_{\theta_{0i}} > \epsilon_{\theta_0}{}^*$, i.e., the maximum occurs after the shell has become locally spherical at the equator, as required. If $\epsilon_{\theta_0}{}^* > (n/2) \times [(2\beta^* + 1)/(\beta^* + 2)]$, the maximum occurs before the shell becomes locally spherical at the equator and therefore must be discarded.

†† Note that, since $\epsilon_{e_0}{}^* = \frac{4}{3}\epsilon_{e_0}{}^* < \frac{2}{3}n$, then $\epsilon_{e_{0i}} > \epsilon_{e_0}{}^*$ as required.

Then, from Eq. (37),

$$p_i = (2HC/R)(\tfrac{2}{3}n)^n e^{-n} \tag{48}$$

This is independent of both β^* and L/R. Interestingly, it is also twice the value for the infinite cylinder. For any $\beta^* \leq 1$ and $\epsilon_{\theta_0}{}^* < n/2$, then,

$$\bar{p}_i = 2 \tag{49}$$

It can be shown that $\bar{p}_i$ as given by Eq. (46) is a nondecreasing function of β^*. For $\beta^* = 1$, Eq. (46) reduces, as expected, to $\bar{p}_i = 2$. In view of this and Eq. (49), then, all values of $\bar{p}_i$ will be contained within an area bounded by the curves for $\beta^* = 1$ and $\beta^* \to \infty$.

As $\beta^* \to \infty$,

$$\bar{p}_i \to 2^{n+1} e^{-\epsilon_{\theta_0}{}^*} \tag{50}$$

Since the critical strain $\epsilon_{\theta_0}{}^*$ is an increasing function of L/R, the pressure ratio in Eq. (50) is a decreasing function of L/R and approaches its maximum as $L/R \to 0$. The greatest "spread" between the results for $\beta^* = 1$ and $\beta^* \to \infty$ also will occur for $L/R \to 0$. If $n = 0.04$,

$$\lim_{L/R \to 0} \bar{p}_i]_{\beta^* \to \infty} = 2.055$$

The entire range of values is shown as the shaded region in Fig. 6. It might be pointed out here that, for $n/2 < \epsilon_{\theta_0}{}^* < n$, the appropriate expression for $\bar{p}_i$ may come either from the foregoing section or from this section, depending on the value of β^*. For example, if $\epsilon_{\theta_0}{}^* = \frac{3}{4}n$, then, for $\beta^* < 4$, Eq. (41) applies, whereas for $\beta^* > 4$, Eq. (46) applies. There is no difficulty as far as continuity is concerned; $\bar{p}_i$ as defined by the set of Eqs. (41, 46, and 49) is continuous in β^*, L/R, and n.

As n increases, the maximum "spread" increases. When $n = 0.10$, the maximum spread is 0.14. The solutions cover an area similar to that for $n = 0.04$ but larger.

Discussion of Results

The results obtained are based on the assumption of a deformed meridian in the shape of a parabola. To the extent that this shape approximates the true shape, the solution approximates the exact solution. Although, as has been pointed out, the assumption of a parabolic meridian is not unreasonable, some further justification of it, and evaluation of the results, is possible.

If the solution were exact, then of course it would satisfy the equilibrium equations (1) and (2). In particular, if Eq. (2) is written in the form

$$p = \frac{\sigma_\theta h}{r_2} \frac{2}{2 - (r_2/r_1)} \tag{51}$$

then substitution into Eq. (51) of the exact expressions for σ_θ, h, r_2, and r_1 as functions of position along the shell's axis should give back the prescribed uniform pressure distribution. If the approximate solution is substituted into Eq. (51), then a pseudopressure can be computed which may be regarded as the pressure associated with the parabolic meridian shape. The deviation of this computed pseudopressure from the uniform is related to the error in the solution. The flatter the computed pressure, the closer is the agreement that can be expected between the instability pressures found and the true values.

Using Eqs. (51, 3–7, 10, 14, 16, and 24), the pressure is obtained as a function of position along the shell's axis:

$$p = \frac{\dfrac{CH}{R}\left(\dfrac{4}{3}\right)^n \left\{\ln\left[1 + \dfrac{w_{0_i}}{R}\left(1 - \dfrac{\zeta^2}{\lambda^2}\right)\right]\right\}^n}{\left[1 + \dfrac{w_{0_i}}{R}\left(1 - \dfrac{\zeta^2}{\lambda^2}\right)\right]^2 \left[1 + \dfrac{4w_{0_i}{}^2}{R^2}\dfrac{R^2}{\lambda^2}\dfrac{\zeta^2}{\lambda^2}\right]^{1/2} \left[1 - \dfrac{w_{0_i}}{R}\dfrac{R^2}{\lambda^2}\dfrac{1 + (w_{0i}/R)(1 - \zeta^2/\lambda^2)}{1 + (4w_{0i}{}^2/R^2)(R^2/\lambda^2)(\zeta^2/\lambda^2)}\right]} \tag{52}$$

Here w_{0_i} is the deflection at the equator at instability and is found easily from Eqs. (6) and (15) once $\epsilon_{\theta_{0i}}$ is known.

Shown in Fig. 7 are the pressure distributions computed at instability for sample first- and second-stage parameter pairs: $n = 0.04$ and $L/R = 1$ in the first stage, and $n = 0.04$ and $L/R = 0.95$ in the second stage. In both distributions, there is a sharp drop-off near the ends of the cylinder. This is because the radial displacement, and therefore the circumferential strain, is taken to be zero at the ends, so that pressure, being proportional to circumferential stress and strain, also must vanish. Over the central half of the shell, the pressure variation is very small in the first stage, being limited to 1%. In the second stage, the variation is somewhat greater—about 10%. The similarity of prescribed and computed distributions would indicate that, at least in the neighborhood of the equator, the assumed shape of the meridian quite closely resembles the true shape for a shell under uniform internal pressure.

In order to judge the sensitivity of results obtained at the equator to changes in meridian shape, parallel developments and solutions were carried out for a circular meridian. Spot numerical checks showed that substitution of this shape for the parabolic changed the pressure ratio by only about 2% when $L/R = 1$, $n = 0.04$, and by about 7% when $L/R = 0.95$, $n = 0.04$.

It is reasonable to expect, then, that the instability pressures obtained are good estimates of the true values appropriate to a shell with a uniform pressure distribution.

Summary

Figures 4 and 6 provide a complete picture of the dependence of the instability pressure on the length-to-radius ratio of cylindrical pressure vessels. For long cylinders ($L/R > 1$), the instability pressure is close to that for the infinite cylinder. For very short cylinders ($L/R \to 0$), the instability pressure is approximately twice the infinite-length value. For cylinders of intermediate length, the instability pressure decreases continuously from the short- to the long-cylinder values. For given L/R, the instability pressure increases with the strain-hardening exponent n. This general behavior confirms the trend of the experimental results presented in Ref. 4.

Overlap of the intermediate-length and long-cylinder curves at L/R values around unity indicates the presence of two local maxima in the pressure-strain curves. The larger local maximum occurs at large strains (25% or more), so that the smaller local maximum may be appropriate for materials of limited ductility.

The existence of discontinuous transitions from first- to second-stage instability pressures apparently is due to use

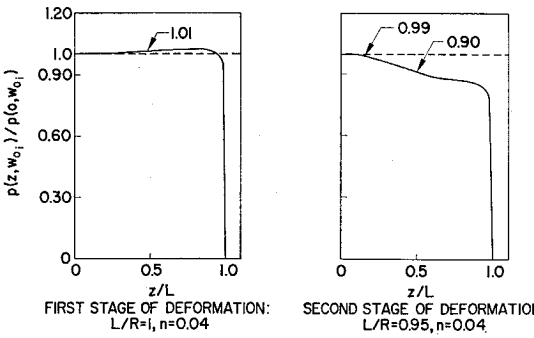

Fig. 7 Pressure distribution associated with assumed parabolic meridian shape

of the piecewise linear Tresca yield condition. It is possible that a continuous solution could be obtained through use of the Mises condition, although it is unlikely that the general shape of the curves in Figs. 4 and 6 would be affected appreciably.

Appendix

The differential equation for $r(\zeta)$ is, from Eqs. (1–14),

$$\frac{pR}{2H}\frac{(\frac{3}{4})^n}{C}\left(\frac{r}{R}\right)^2[2(1+r'^2)+r\,r'']-\left[\ln\left(\frac{r}{R}\right)\right]^n(1+r'^2)^{1/2}=0 \quad \text{(A1)}$$

where $R = R + w$, $r' = w'$.

If the restriction is imposed that

$$w/R \ll 1 \quad \text{(A2)}$$

$$w'^2 \ll 1 \quad \text{(A3)}$$

then Eq. (A1) simplifies to

$$\frac{pR}{2H}\frac{(\frac{3}{4})^n}{C}[2+Rw'']-\left(\frac{w}{R}\right)^n=0 \quad \text{(A4)}$$

The first integral of (A4) is

$$\frac{pR}{2H}\frac{(\frac{3}{4})^n}{C}[2w+\tfrac{1}{2}Rw'^2]-\frac{R}{n+1}\left(\frac{w}{R}\right)^{n+1}=C_1 \quad \text{(A5)}$$

The constant of integration is obtained from the condition that $w' = 0$ at $w = w_{max}$, since the maximum value of w cannot occur at the ends of the shell. Equation (A5) may be written as

$$\eta'^2 = (4/w_{max}R)[(1-\eta)-k(1-\eta^{n+1})] \quad \text{(A6)}$$

where

$$k \equiv \frac{CH(w_{max}/R)^n}{(\frac{3}{4})^n(n+1)pR} \quad \text{(A7)}$$

$$0 \le \eta \equiv w/w_{max} \le 1 \quad \text{(A8)}$$

From the definition of η, and since $n > 0$,

$$\frac{1}{n+1} < \frac{1-\eta}{1-\eta^{n+1}} \le 1 \quad \text{(A9)}$$

Since one must have $\eta'^2 \ge 0$, k is restricted so that

$$k \le 1/(n+1) \quad \text{(A10)}$$

The function η'^2 as defined by Eq. (A6) is monotonic decreasing in η for $0 \le \eta \le 1$. It has only one zero in the interval $0 \le \eta \le 1$, and that occurs at $\eta = 1$. Because of symmetry requirements for the deformed meridian, there must be a zero of w', and therefore of η', at $\zeta = 0$. Since η' has a zero only at $\eta = 1$, one must have $\eta = 1$ at $\zeta = 0$, i.e., the maximum displacement occurs at the equator and $w_{max} = w_0$. Also, since there is a relative maximum but no relative minimum, η must be positive for $\zeta < 0$ and negative for $\zeta > 0$.

Because of Eq. (A9),

$$[1-(\eta+1)k](1-\eta) \le [(1-\eta)-k(1-\eta^{n+1})] \le [(1-k)(1-\eta)] \quad \text{(A11)}$$

Therefore, going back to Eq. (A6) and considering, e.g., $\zeta < 0$, $\eta' > 0$,

$$\left[\frac{1-(n+1)k}{w_0R}\right]^{1/2} \le \frac{\eta'}{2(1-\eta)^{1/2}} \le \left(\frac{1-k}{w_0R}\right)^{1/2} \quad \text{(A12)}$$

On integrating and using the fact that $\eta = 1$ at $\zeta = 0$, one obtains

$$\left[\frac{1-(n+1)k}{w_0R}\right]^{1/2}\zeta \le (1-\eta)^{1/2} \le \left(\frac{1-k}{w_0R}\right)^{1/2}\zeta \quad \text{(A13)}$$

This means that for fixed w_0 the solution is bounded below by the parabola

$$\eta_1 = 1 - [(1-k)/w_0R]\zeta^2 \quad \text{(A14)}$$

with axial half-length

$$\lambda_1 = [w_0R/(1-k)]^{1/2} \quad \text{(A15)}$$

and that the solution is bounded above the parabola

$$\eta_2 = \{[1-(n+1)k]/w_0R\}\zeta^2 \quad \text{(A16)}$$

with axial half-length

$$\lambda_2 = \left[\frac{w_0R}{1-(n+1)k}\right]^{1/2} \quad \text{(A17)}$$

Equation (A7), together with Eq. (A15) or (A17), provides an expression for the pressure in terms of w_0:

$$\left(\frac{3}{4}\right)^n\frac{pR}{CH} = \frac{(w_0/R)^n}{(n+1)[1-(R/\lambda_1)^2(w_0/R)]} = \frac{(w_0/R)^n}{[1-(R/\lambda_2)^2(w_0/R)]} \quad \text{(A18)}$$

This satisfies the requirement of Eq. (A10) that

$$(\tfrac{3}{4})^n(pR/CH) \ge (w_0/R)^n$$

The pressure as given by Eq. (A18) is an increasing function of w_0, so that no maximum in p is observed as long as $w_0/R \ll 1$, $w'^2 \ll 1$.

A more exact form of the solution, free of these restrictions, would be required in order to show the development of the maximum pressure. For sufficiently short shells, it is possible that the shell will become locally spherical at the equator while (A2) and (A3) still are satisfied. Equation (A1) then must be replaced with one appropriate to $r_2/r_1 \ge 1$.

Although the solutions given here are not appropriate for large pressures or displacements, they do provide a reasonable estimate of the pressure-displacement relationship and meridian shape at the beginning of the deformation process.

References

[1] Hoffman, O. and Sachs, G., *Introduction to the Theory of Plasticity for Engineers* (McGraw-Hill Book Co., Inc., New York, 1953), pp. 148–162.

[2] Fraser, A. F. and Jablonski, H., "Plastic instability of finite cylinders," TD-13, Aerojet-General Corp., Sacramento, Calif. (January 1961).

[3] Weil, N. A., "An approximate solution for the bursting of thin-walled cylinders with a finite L/D ratio," ARF 4132-17, Armour Research Foundation, Chicago (rough draft).

[4] Sachs, G., Schapiro, L., and Hoffman, O., "Strength of ductile metal motor cases," TR 6-90-61-9, Lockheed Missiles & Space Co., Sunnyvale, Calif. (June 1961).